PERGAMON

International Journal of Heat and Mass Transfer 43 (2000) 3925–3936

International Journal of HEAT and MASS TRANSFER

www.elsevier.com/locate/ijhmt

Heat transfer for water flow in trapezoidal silicon microchannels

Weilin Qu, Gh. Mohiuddin Mala, Dongqing Li*

Department of Mechanical Engineering, University of Alberta, Edmonton, AB, Canada, T6G 2G8

Received 23 November 1999; received in revised form 26 January 2000

Abstract

Experiments were conducted to investigate heat transfer characteristics of water flowing through trapezoidal silicon microchannels with a hydraulic diameter ranging from 62 to 169 μm. A numerical analysis was also carried out by solving a conjugate heat transfer problem involving simultaneous determination of the temperature field in both the solid and the fluid regions. The experimental results were compared with the numerical predictions and a significant difference was found. The comparison results indicated that the experimentally determined Nusselt number is much lower than that given by the numerical analysis. The measured lower Nusselt numbers may be due to the effects of surface roughness of the microchannel walls. Based on a roughness-viscosity model established in our previous work, a modified relation which accounts for the roughness-viscosity effects was proposed to interpret the experimental results. © 2000 Elsevier Science Ltd. All rights reserved.

1. Introduction

The rapid development and wide application of high performance very large-scale integration (VLSI) technology result in significant improvement in the performance of electronic and microelectronic devices. However, with the improvement of circuit density and operating speed, more heat is generated by the electronic systems. Since most operating parameters of the components are related to their temperature, thermal management of high power density electronic systems has become one of the most important aspects in electronic industry in recent years. Microchannel heat exchangers or microchannel heat sinks may provide efficient cooling for these high power density applications.

The concept of the microchannel heat sinks was first introduced by Tuckermann and Pease [15]. They demonstrated that the microchannel heat sinks, consisting of microrectangular flow passages, have a higher heat transfer coefficient in laminar flow regime than that in turbulent flow through macrosize channels. Therefore, a significantly high heat flux can be dissipated by using such a microchannel heat sink. A detailed review of the research works on microchannel heat sinks can be found elsewhere [11].

Effective design of the microchannel heat sinks requires fundamental understanding of the characteristics of heat transfer and fluid flow in microchannels and in microchannel structures. At the early stage of the designs, the relationships of macroscale fluid flow and heat transfer were employed. However, many experimental observations have shown that the heat transfer behaviors in microchannels

* Corresponding author. Tel.: +1-403-492-9734; fax: +1-403-492-2200.

E-mail address: dongqing.li@ualberta.ca (D. Li).

0017-9310/00/$ - see front matter © 2000 Elsevier Science Ltd. All rights reserved.
PII: S0017-9310(00)00045-4

Nomenclature

A	coefficient in Eq. (24)
A_c	cross-sectional area of the microchannel
A_w	total area of the side wall and the bottom wall of the microchannel
DIUF	deionized ultra-filtered water
L_1	width of the unit cell
L_2	thickness of the microchannel plate
L_3	length of the microchannel
N	number of microchannels per plate
Nu	Nusselt number
P	pressure
ΔP	pressure drop across the microchannel
Q	total heat removed by water
R_h	hydraulic radius of the microchannel, which is the half of the hydraulic diameter d_h
Re	Reynolds number
Re_k	Reynolds number based on the roughness
S	source term
T	temperature
T_1, T_2, T_3	longitudinal wall temperature of the microchannel plate
T_{in}, T_{out}	inlet and outlet water temperature
T_m	fluid bulk mean temperature
T_{wm}	mean temperature along the bottom wall of the unit cell
ΔT_m	mean temperature difference between water and microchannel wall
V	volume flow rate
W	nondimensional velocity
W_k	velocity at the top of the roughness element
W_m	mean nondimensional velocity
X, Y, Z	nondimensional Cartesian coordinates
a, b, h	dimensions of the trapezoidal microchannel
c_P	specific heat
d_h	hydraulic diameter of the channel, that is, ratio of four times the cross-sectional area to the wetted perimeter of the channel
h_f	average heat transfer coefficient
l	length of the side wall of the microchannel
l_{min}	shortest distance from the point to the microchannel wall
k	height of the roughness element
n	outer normal coordinate at a point on the microchannel wall inside periphery Γ
q	heat flux at the bottom wall of the microchannel plate
w	velocity in the z direction
w_m	mean velocity
w_x	uncertainty of variable x
x, y, z	Cartesian coordinates

Greek symbols

λ	thermal conductivity
μ	dynamic viscosity
μ_{app}	apparent viscosity
μ_R	roughness viscosity
μ_{Rm}	mean roughness viscosity
μ_{Rmw}	mean roughness viscosity near the wall
θ	nondimensional temperature
θ_{wm}	mean nondimensional temperature along the bottom wall of the unit cell
ρ	density
τ	arbitrary transport property
Γ	inside periphery of the microchannel wall

Subscripts

exp	experimental
f	fluid
g	Pyrex glass
s	silicon
thy	theoretical
w	wall
R	roughness

deviate significantly from those in macroscale channels.

Wu and Little [17] measured the heat transfer characteristics for gas flows in miniature channels with inner diameter ranging from 134 to 164 μm. The tests involved both laminar and turbulent flow regimes. Their results showed that the turbulent convection occurs at Reynolds number of approximately 1000. They also found that the convective heat transfer characteristics depart from the predictions of the established empirical correlations for macroscale tubes. They attributed these deviations to the asymmetric roughness and the large relative roughness of the microchannel walls.

Choi et al. [2] measured the convective heat transfer coefficients for flow of nitrogen gas in microtubes for both laminar and turbulent regimes. The internal diameter of these microtubes ranges from 3 to 81 μm.

They found that the measured Nusselt number in laminar flow exhibits a Reynolds number dependence, in contrast to the conventional prediction for fully developed laminar flow, in which Nusselt number is constant. In turbulent flow, the measured Nusselt numbers are larger than those predicted by the Dittus–Boelter correlation and the Colburn analogy is no longer valid. No early transition to turbulent convection was observed.

Wang and Peng [16] experimentally investigated the convection of water and methanol through microchannels with rectangular cross-sections. The hydraulic diameter of the microchannels ranges from 311 to 747 μm. They found that the liquid convection characteristics are quite different from those of the conventional cases. In laminar flow regime, the relationship between Nusselt number and Reynolds number is quite complex, and Nusselt number is a function of other parameters in addition to Reynolds number. A fully developed turbulent convection occurs at $Re =$ 1000–1500. The fully developed turbulent heat transfer can be predicted by the Dittus–Boelter correlation by modifying the empirical constant coefficients. The characteristics of convective heat transfer are strongly affected by liquid temperature, velocity and microchannel size.

Yu et al. [18] studied the convective heat transfer characteristics of water in microtubes with diameters of 19, 52, and 102 μm. The experiments were performed for turbulent regimes with Reynolds number greater than 2500. It was found that at a low Reynolds number, the heat transfer data from microtubes and large tubes are more or less same, but the values diverge as the Reynolds number increases. Values of Nusselt number are always higher than those predicted by the conventional correlations. The Colburn correlation is invalid and Colburn factor changes with the Reynolds number.

Peng and Peterson [9] investigated the single-phase forced convective heat transfer of water in microchannel structure/plates with rectangular channels. The hydraulic diameter of the microchannels changes from 133 to 367 μm. Their results indicated that the Reynolds number for transition from laminar to turbulent flow become much smaller than that for flow in the ordinary channels. The aspect ratio of the channel cross-section has a significant effect on the convective heat transfer. Empirical correlations were suggested for prediction of the heat transfer for both laminar and turbulent regimes.

Adams et al. [1] experimentally investigated the turbulent convective heat transfer of water in microtubes with inner diameters of 760 and 1090 μm. Their results showed that Nusselt number for the microtubes is higher than that predicted by the conventional empirical correlations for macroscale tubes. A generalized correlation for Nusselt number for single-phase forced turbulent convection in microtubes was proposed.

Our current understanding of the special heat transfer behaviors in microchannels is far from sufficient. It is necessary to carry out fundamental investigations to understand the difference between the experimental data and the conventional heat transfer theory and correlations. In practice, the cross-section of microchannels made by modern micromachining technology (e.g., anisotropic chemical etching) in silicon substrates is essentially trapezoidal. The objective of this work is to experimentally investigate the heat transfer characteristics of water in trapezoidal microchannels made of silicon plates and to attempt to explain the experimental results.

2. Experimental setup and procedure

A schematic of the experimental apparatus used to investigate heat transfer characteristics of water in trapezoidal silicon microchannels is shown in Fig. 1. Deionized ultra filtered water (DIUF) (Fisher Scientific) was used as the working fluid. Water was pumped from the liquid reservoir by a high precision pump (Ruska Instruments, Model: 2248-WII) which has a flow rate range of 2.5–560 cm^3/h and can generate a pressure up to 4000 psi. In order to avoid any particles or bubbles from flowing through and blocking the microchannels, a 0.1 μm filter was installed between the outlet of the pump and the inlet of the microchannels, and water was forced to flow through the submicron filter before entering the microchannels. The volume flow rate of water flowing through the microchannels was measured by a precision flowmeter (Chem Tec Equipment Co., Model: MAO-125 AA). The flowmeter is designed for low flow rate (up to 70 cm^3/min) and was calibrated by the

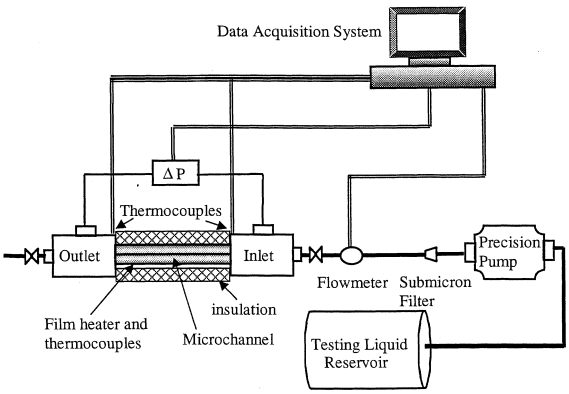

Fig. 1. Schematic of the experimental system for measuring heat transfer characteristics of water flow in microchannels.

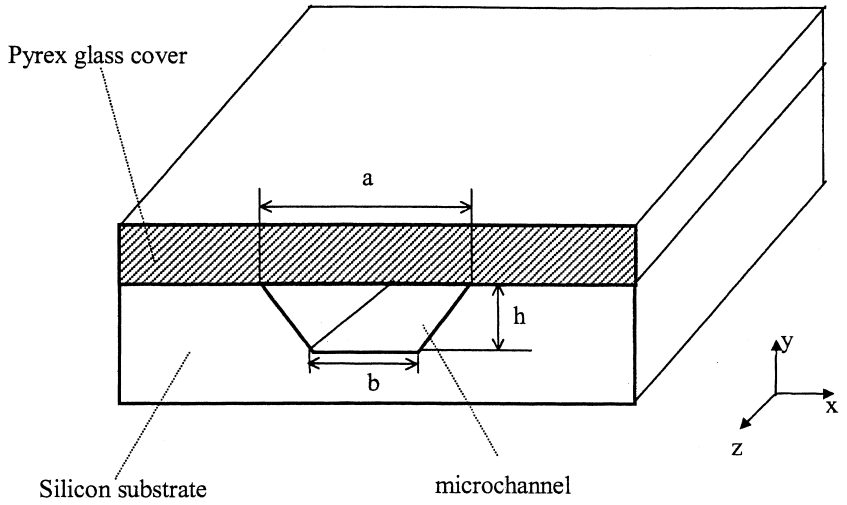

Fig. 2. Schematic of a trapezoidal microchannel in a silicon plate with a Pyrex glass cover.

standard weighing method as follows. Basically, the liquid exiting the channel was accumulated in a glass beaker. An electronic balance (Mettler Instrumente AG, Model: BB240) with an accuracy of 0.001 g was used to measure the weight of the accumulated liquid. The volume of the liquid was determined by dividing the weight by the liquid's density. Details of the calibration are given in Mala [19]. The accuracy of the flow rate measurement was estimated to be 2%.

The trapezoidal silicon microchannels used in this work were fabricated by anisotropic etching technique at the Alberta Microelectronic Center (Edmonton, Canada). First several microslots were etched in a silicon plate and then a Pyrex glass cover was anodically bonded on the top of the plate. The microchannel plates used in the measurement have a dimension of $30 \times 10 \times 1$ mm, where the thickness of the silicon substrate is 0.4 mm and that of the Pyrex glass cover is 0.6 mm. There are five microchannels in each plate. All the microchannels in one plate have the same dimensions so that the flow through each channel is identical. The cross-section of such a microchannel is illustrated in Fig. 2. The dimensions of the microchannels were measured by a microscope (Leica MS5 Stereomicroscope)-computer image analysis system with a resolution of 0.8 μm. The characteristic sizes are listed in Table 1. The hydraulic diameter of the microchannels used in this study ranges from 62 to 169 μm.

The microchannel plate was placed in a two-part symmetrical Plexiglas assembly, as shown in Fig. 3. The epoxy resin was used to bond the microchannel plate and the assembly together to avoid leaking. Two sumps were machined in the assembly and were connected by the microchannels. A diaphragm type differential pressure transducer (Validyne Engineering, Model: DP15) with ±0.5% FS accuracy was connected to the sumps to measure the pressure drop along the microchannels.

A film heater was attached on the bottom wall (silicon) of the microchannel plate. A thermal compound (Wakefield Engineering) was employed to fill the vacant spaces between the bottom wall of the microchannel plate and the film heater in order to reduce the thermal contact resistance. The microchannel plate was electrically heated by connecting the film heater to a power source which can provide low electric voltage and high current. As a result of Joule heating, the thermal boundary condition on the bottom wall of the microchannel plate approximates a constant heat flux condition. The test section consisting of the microchan-

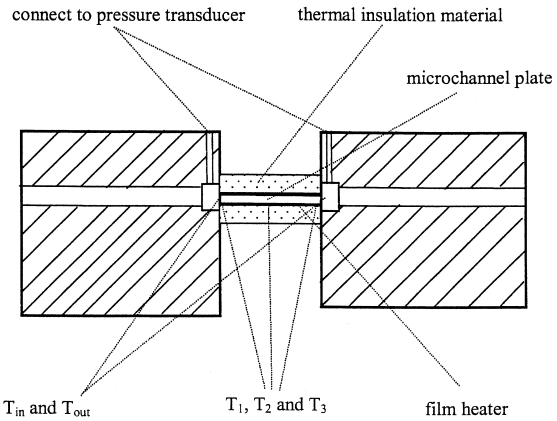

Fig. 3. Schematic of the test section.

Table 1
Characteristic dimensions of the trapezoidal silicon microchannels[a]

Channel No.	a (μm)	b (μm)	h (μm)	d_h (μm)	Average roughness, k (μm)
1	148.33	94.83	44.44	62.3	0.8
2	408.23	348.17	35.41	63.1	0.8
3	237.01	66.11	109.77	114.5	2.0
4	523.20	356.32	111.14	168.9	2.0

[a] Length of the microchannels $L_3 = 3.0$ cm and number of microchannels per plate-5.

nel plate and the film heater was well insulated by thermal insulation materials to minimize heat loss to the surrounding through convection and radiation. Three 127 μm copper–constantan (type T) thermocouples (Omega Engineering, Model: 5TC-TT-T-36-36) were mounted on the bottom wall of the microchannel plate along the flow direction to measure the longitudinal wall temperature distribution. Two copper–constantan thermocouples (Omega Engineering, Model: 5TC-TT-T-36-36) were placed at the ends of the microchannel to measure the inlet and outlet temperatures of water. The thermocouples were calibrated by the standard comparison method used before in the experiment. The details of the calibration procedures and the results are given in Mala's Ph.D. Thesis [19]. The accuracy of the temperature measurement is estimated to be $\pm 0.3^{\circ}$C.

All the measurement devices were connected to a computer data acquisition system. During a measurement, the pump, as well as the power source, were set to maintain a desired output. The pump was set to produce a constant flow rate at a steady state. The output of the power source was so set as to obtain desired temperature distributions. For example, the maximum longitudinal wall temperature difference of the microchannel plates, $T_3 - T_1$, was less than 30°C; the temperature difference of water at the inlet and outlet, $T_{out} - T_{in}$, was also less than 30°C; and the temperature difference between the water and the microchannel plates was less than 10°C. The temperatures and the pressure drop along the microchannel were measured. For each measurement, the flow was considered to have reached a steady state when the readings of the temperatures and the pressure drop did not change any more. At such a steady state, the temperatures, the pressure drop and the flow rate were monitored and recorded for about 30 min. The data reported in this paper are for steady states. The measurement for the same microchannel was repeated at least twice for the same flow rate. Then the pump and the power source were set to different outputs and another set of measurement was conducted for the same microchannel. For every microchannel, the test was conducted up to a pressure drop of 250 psi, as microchannel failure (breaking) usually occurred at pressures drop greater than 250 psi. Therefore, this limited the Reynolds number range to only a few hundreds for smaller microchannels.

The uncertainties involved in the measurements were analyzed and evaluated. The results are given in Table 2. The detailed experimental uncertainty analysis can be found in Appendix A. For graphic reasons, the error bars were not shown in all the plots reported in this paper.

3. Results and discussion

In this section, the heat transfer in the microchannel plates is first analyzed numerically by solving a conjugate problem involving simultaneous determination of the temperature field in both the fluid and the solid regions. Then the experimental results are analyzed and compared with the results of the numerical analysis. Finally, based on a roughness-viscosity model developed in our previous work [13], a modified relationship is proposed to interpret the observed special heat transfer behaviors in the microchannels.

3.1. Numerical analysis

As the ratios of length to hydraulic diameter of the microchannels are very large and Reynolds number is relatively low, we neglect the entrance effects and assume a laminar, fully developed (hydraulically and thermally) flow in the trapezoidal microchannels. Taking advantage of symmetry, we choose a unit cell

Table 2
Experimental uncertainties

Parameters	Uncertainty (%)
Flow rate	2.0
Pressure drop	1.0
Temperatures	0.8
Reynolds number	4.6
Nusselt number	8.5

as consisting of half a channel and the surrounding solid as shown in Fig. 4. The thermal boundary condition at the bottom boundary is the constant heat flux boundary condition and at the top boundary is the adiabatic boundary condition because the top wall is well insulated by thermal insulation materials. Due to the symmetry, the two side boundaries of the unit cell also have the adiabatic boundary conditions. The heat transport in the unit cell is a conjugate problem which combines heat conduction in the solid region (silicon and glass) and heat convection in the fluid region. Since the temperature distribution in the fluid is coupled with that in the solid, in order to determine the heat transfer characteristics in the unit cell, the conduction in the solid region need to be solved simultaneously with the convection in the fluid. The application of the finite difference method on the conjugated problems was discussed in details by Patankar [8]. Basically, the whole unit cell is chosen as the computation domain. The momentum equation is solved in a usual manner by assigning the true value to the viscosity in the fluid and a very large value to the viscosity in the solid region. In this way, if a zero velocity is specified as the boundary condition of the computation domain, the high viscosity in the solid will establish a zero velocity throughout the solid region, thus providing the appropriate boundary condition to the fluid region. If the material properties of the system are constant, once the velocity field is determined, the energy equation can be solved after specifying the thermal conductivities for the fluid and solid regions.

At steady state and in the absence of thermal energy sources, viscous dissipation and axial heat conduction, the governing differential equations in the unit cell can be expressed as follows.

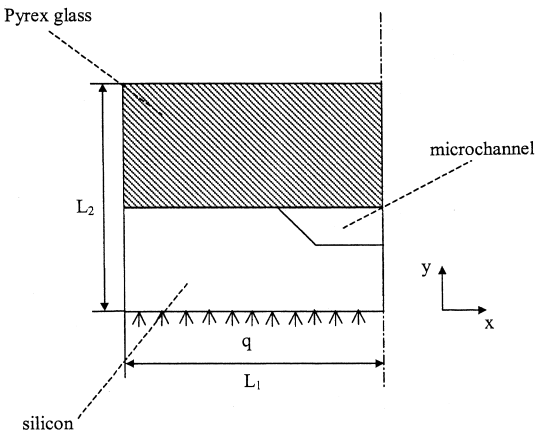

Fig. 4. Schematic of a unit cell in the microchannel plate for numerical analysis.

In the liquid region, the momentum equation is written as

$$\frac{\mathrm{d}P}{\mathrm{d}z} = \mu_{\mathrm{f}}\left(\frac{\partial^2 w}{\partial x^2} + \frac{\partial^2 w}{\partial y^2}\right) \tag{1}$$

The energy equation is

$$\rho_{\mathrm{f}} c_{\mathrm{Pf}} w \frac{\partial T}{\partial z} = \lambda_{\mathrm{f}}\left(\frac{\partial^2 T}{\partial x^2} + \frac{\partial^2 T}{\partial y^2}\right) \tag{2}$$

Since the flow is fully developed, one has

$$\frac{\partial T}{\partial z} = \frac{\mathrm{d}T_{\mathrm{m}}}{\mathrm{d}z} \tag{3}$$

where T_{m} is the fluid bulk mean temperature and defined as

$$T_{\mathrm{m}} = \frac{1}{A_{\mathrm{c}} w_{\mathrm{m}}} \int_{A_{\mathrm{c}}} wT \,\mathrm{d}A_c \tag{4}$$

and w_{m} is the fluid mean velocity,

$$w_{\mathrm{m}} = \frac{1}{A_{\mathrm{c}}} \int_{A_{\mathrm{c}}} w \,\mathrm{d}A_{\mathrm{c}} \tag{5}$$

From the energy conservation along the microchannels, one has

$$\rho_{\mathrm{f}} c_{\mathrm{Pf}} w_{\mathrm{m}} A_{\mathrm{c}} \frac{\mathrm{d}T_{\mathrm{m}}}{\mathrm{d}z} \mathrm{d}z = qL_1 \,\mathrm{d}z \tag{6}$$

By substituting Eqs. (3) and (6) into Eq. (2), the energy equation can be rewritten as

$$\frac{qL_1}{A_{\mathrm{c}}}\left(\frac{w}{w_{\mathrm{m}}}\right) = \lambda_{\mathrm{f}}\left(\frac{\partial^2 T}{\partial x^2} + \frac{\partial^2 T}{\partial y^2}\right) \tag{7}$$

In the solid region, the energy equation is written as

$$\lambda_{\mathrm{s}}\left(\frac{\partial^2 T}{\partial x^2} + \frac{\partial^2 T}{\partial y^2}\right) = 0 \tag{8a}$$

in the silicon substrate and

$$\lambda_{\mathrm{g}}\left(\frac{\partial^2 T}{\partial x^2} + \frac{\partial^2 T}{\partial y^2}\right) = 0 \tag{8b}$$

in the Pyrex glass cover.

Nondimensionlize the governing equations, Eqs. (1) and (7)–(8b), by means of the following nondimensional parameters

$$X=\frac{x}{d_h},\quad Y=\frac{y}{d_h},\quad W=\frac{\mu_f w}{-d_h^2(\mathrm{d}P/\mathrm{d}z)},\quad \theta=\frac{T-T_m}{(qd_h/\lambda_f)} \tag{9}$$

After some rearrangement, the nondimensionalized governing equations in fluid and solid regions can be expressed as a unified form. The momentum equation in the computation domain is written as

$$\frac{\partial}{\partial X}\left(\overline{\mu}\frac{\partial W}{\partial X}\right)+\frac{\partial}{\partial Y}\left(\overline{\mu}\frac{\partial W}{\partial Y}\right)+S_w=0 \tag{10a}$$

where in solid region

$$\overline{\mu}=10^{30},\quad S_w=0 \tag{10b}$$

and in fluid region

$$\overline{\mu}=1,\quad S_w=1 \tag{10c}$$

The energy equation is

$$\frac{\partial}{\partial X}\left(\overline{\lambda}\frac{\partial \theta}{\partial X}\right)+\frac{\partial}{\partial Y}\left(\overline{\lambda}\frac{\partial \theta}{\partial Y}\right)+S_\theta=0 \tag{11a}$$

where in solid region

$$\overline{\lambda}=\frac{\lambda_s}{\lambda_f}\ \text{or}\ \frac{\lambda_g}{\lambda_f},\quad S_\theta=0 \tag{11b}$$

and in fluid region

$$\overline{\lambda}=1,\quad S_\theta=-\frac{L_1 d_h}{A_c}\left(\frac{W}{W_m}\right) \tag{11c}$$

The boundary conditions for Eqs. (10a)–(11c) are shown in Fig. 5.

A finite difference scheme is applied to Eqs. (10a)–(11c) and the resulting system of algebraic equations is solved using the Gauss–Seidal iterative technique, with successive over-relaxation employed to improve the convergence time. It should be noted that some special numerical techniques are employed in the calculations. For example, the harmonic mean method is used to handle the large discontinuities of nondimensional viscosity and thermal conductivity at the solid–fluid interfaces. In this method, the transport property at the interface is evaluated by

$$\tau_{i+1/2}=\frac{2\tau_i\tau_{i+1}}{\tau_i+\tau_{i+1}}, \tag{12}$$

rather than by the arithmetic mean. The step succession method is used to handle the irregular shape of the trapezoidal microchannels. Successive steps are chosen to accommodate the side wall of the channel as shown in Fig. 5. The detailed description of these numerical techniques can be found elsewhere [7,12].

The nondimensional temperature distribution in the microchannel plates used in our experiments is computed. In the calculations, the thermal conductivities of the silicon substrate, the glass cover plate and the water take the values of 148, 1.13, and 0.607 W/(m K), respectively. As an example, the temperature contour map for the microchannel plate with 169 μm channel inner diameter of 169 μm is shown in Fig. 6. It can be seen from the figure that the boundary between the solid and the fluid is clearly visible due to a large change in the temperature gradient at the interface. Due to the silicon's high thermal conductivity, the temperature gradient in the silicon substrate is very small and the temperature field is close to an isothermal one. Therefore, it is safe to use the bottom wall temperature of the microchannel plates to represent the temperature

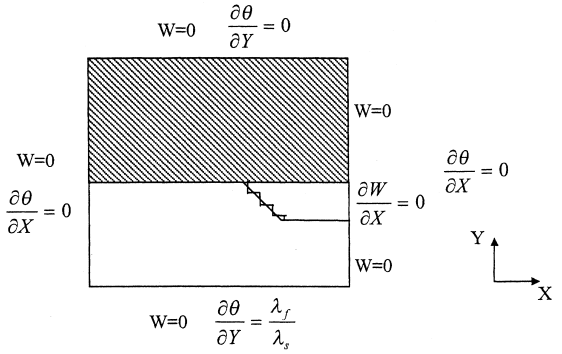

Fig. 5. Schematic of the computation domain.

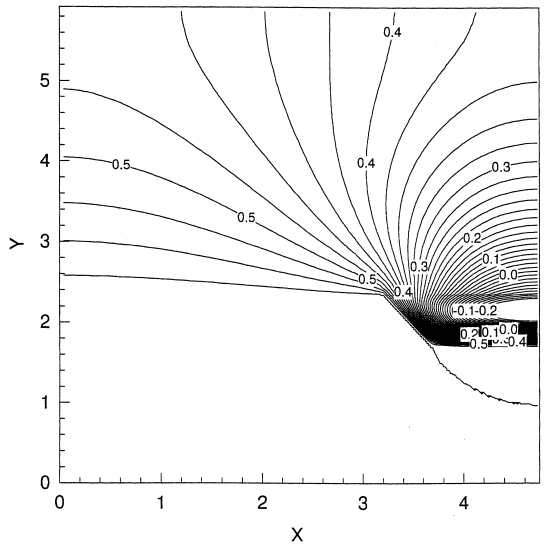

Fig. 6. Nondimensional temperature contour map for the unit cell (Fig. 4) in microchannel plate. The hydraulic diameter of the microchannel is 169 μm.

along the side wall and the bottom wall of the microchannel. As can be seen in Fig. 6, the temperature gradient perpendicular to the top boundary of the microchannel is small as compared to the gradient along the side and the bottom boundaries. As mentioned before, the thermal conductivity of the Pyrex glass cover is about two orders of magnitude smaller than that of the silicon substrate. Therefore, the heat transport through the top boundary of the microchannel should be much smaller than that through the side and the bottom boundaries.

Based on the discussion above, we defined the average Nusselt number of the microchannels as

$$Nu_{\mathrm{thy}} = \frac{qL_1}{l+(b/2)} \frac{d_{\mathrm{h}}}{(T_{\mathrm{wm}} - T_{\mathrm{m}})\lambda_{\mathrm{f}}} \tag{13}$$

where T_{wm} is the mean temperature along the bottom wall of the microchannel plate.

$$T_{\mathrm{wm}} = \frac{1}{L_1} \int_{L_1} T \, \mathrm{d}x \tag{14}$$

By means of the nondimensional temperature, Nusselt number can be rewritten as

$$Nu = \frac{L_1}{l+(b/2)} \frac{1}{\theta_{\mathrm{wm}}} \tag{15}$$

where

$$\theta_{\mathrm{wm}} = \frac{1}{\overline{L}_1} \int_{\overline{L}_1} \theta \, \mathrm{d}X \tag{16}$$

3.2. Experimental data reduction

During the experiments, the measured parameters were the total volume flow rate V, the pressure drop across the microchannels ΔP, the bottom wall (silicon) temperatures of the microchannel plate from upstream to downstream, T_1, T_2 and T_3, and the inlet and outlet water temperatures T_{in} and T_{out}. Other parameters used to describe the heat transfer and fluid flow characteristics of water are related to these measured parameters. For example, the Reynolds number can be evaluated by

$$Re = \frac{\rho_{\mathrm{f}} V d_{\mathrm{h}}}{N A_{\mathrm{c}} \mu_{\mathrm{f}}} \tag{17}$$

and the average Nusselt number is determined by

$$Nu_{\mathrm{exp}} = \frac{h_{\mathrm{f}} d_{\mathrm{h}}}{\lambda_{\mathrm{f}}} \tag{18}$$

where h_{f} indicates the average heat transfer coefficient along the microchannel wall and is calculated by

$$h_{\mathrm{f}} = \frac{Q}{N A_{\mathrm{w}} \Delta T_{\mathrm{m}}} \tag{19}$$

The parameters in Eq. (19) are specified as follows. Q is the heat removed by water. At steady state, if the heat loss through the thermal insulation materials is neglected, the heat generated by the film heater is totally removed by the water flowing through the microchannels. From energy conservation, Q can be evaluated by

$$Q = \rho_{\mathrm{f}} c_{\mathrm{Pf}} V (T_{\mathrm{out}} - T_{\mathrm{in}}) \tag{20}$$

A_{w} is the total area of the side and bottom walls of the microchannel.

$$A_{\mathrm{w}} = (2l + b) \cdot L_3 \tag{21}$$

ΔT_{m} is the mean temperature difference between the water and the bottom wall of the microchannel plate and is evaluated by

$$\Delta T_{\mathrm{m}} = \frac{1}{3}(T_1 + T_2 + T_3) - \frac{1}{2}(T_{\mathrm{in}} + T_{\mathrm{out}}) \tag{22}$$

It is apparent that the average Nusselt number determined from Eq. (18) is in accordance with the one defined in Eq. (13).

The mean water temperature $\frac{1}{2}(T_{\mathrm{in}} + T_{\mathrm{out}})$ is used as the characteristic temperature to determine all physical properties of water involved in these calculations, such as density ρ_{f}, dynamic viscosity μ_{f}, thermal conductivity λ_{f}, and specific heat c_{Pf}. These parameters are assumed to be independent of the pressure.

3.3. Nusselt number

For all the microchannels used in this study, the experimental Nusselt number is plotted in Fig. 7a–d as a function of the Reynolds number. For the purpose of comparison, the results predicted by the numerical calculation are also plotted in Fig. 7a–d. As seen in figures, the numerical Nusselt numbers are constant as required by the conventional heat transfer theory. The experimental Nusselt numbers for all the microchannels are also approximately constant. The Reynolds number dependence of the Nusselt number is not apparent. It can be clearly seen that all experimental data fall below the values predicted by the numerical analysis. This means that at a given Reynolds number, the convection in the microchannels has a lower heat transfer coefficient than the prediction of the conventional heat transfer theory.

3.4. Roughness-viscosity model

The above discussed deviation between the experimentally determined Nusselt number and that pre-

dicted by the conventional theory may be caused by the surface roughness and the micron dimensions. We measured the surface roughness of the microchannels. The surface roughness of the Pyrex glass covers was measured by a Tencor Surface Profilemeter (TSP). It was found that the surfaces of the Pyrex glass covers are very smooth and the average surface roughness is of the order of 10 nm. The average surface roughness of the silicon surface was measured by a high resolution inverted research metallurgical microscope (Olympus, Model: PMG3). The roughness k varies approximately from 0.8 μm for smaller microchannels to 2 μm for larger microchannels, as shown in Table 1. The roughness of such an order of magnitude can be safely neglected if the dimensions of the flow channel are above the order of millimeters. However, for microchannels used in this study, the ratio $2k/d_h$ ranges from 2.4 to 3.5%. The channels height is the smallest dimension for these trapezoidal microchannels. As seen from Table 1, the ratio $2k/h$ ranges from 3.5 to 4.5%. Therefore, the surface roughness may have profound effects on the velocity field and the heat transfer in microchannels.

Generally, the presence of the surface roughness will influence the momentum transfer near the wall, which will further affect the laminar velocity profile. This has been shown by a number of experiments and a comprehensive review can be found elsewhere [6,14]. Based on Merkle et al.'s modified-viscosity model [6], Mala and Li [4] suggested a roughness-viscosity model which accounts for this additional momentum transfer by introducing a roughness-viscosity μ_R in a manner similar to the eddy-viscosity concept in the turbulent flow model. In this way, the apparent viscosity of the fluid becomes the sum of the fluid viscosity and the roughness viscosity, which is

$$\mu_{app} = \mu_R + \mu_f \tag{23}$$

The roughness viscosity was applied to explain the effects of the surface roughness on laminar flow in microtubes. Qu et al. [13] further applied this model to explain the special flow behaviors of water in

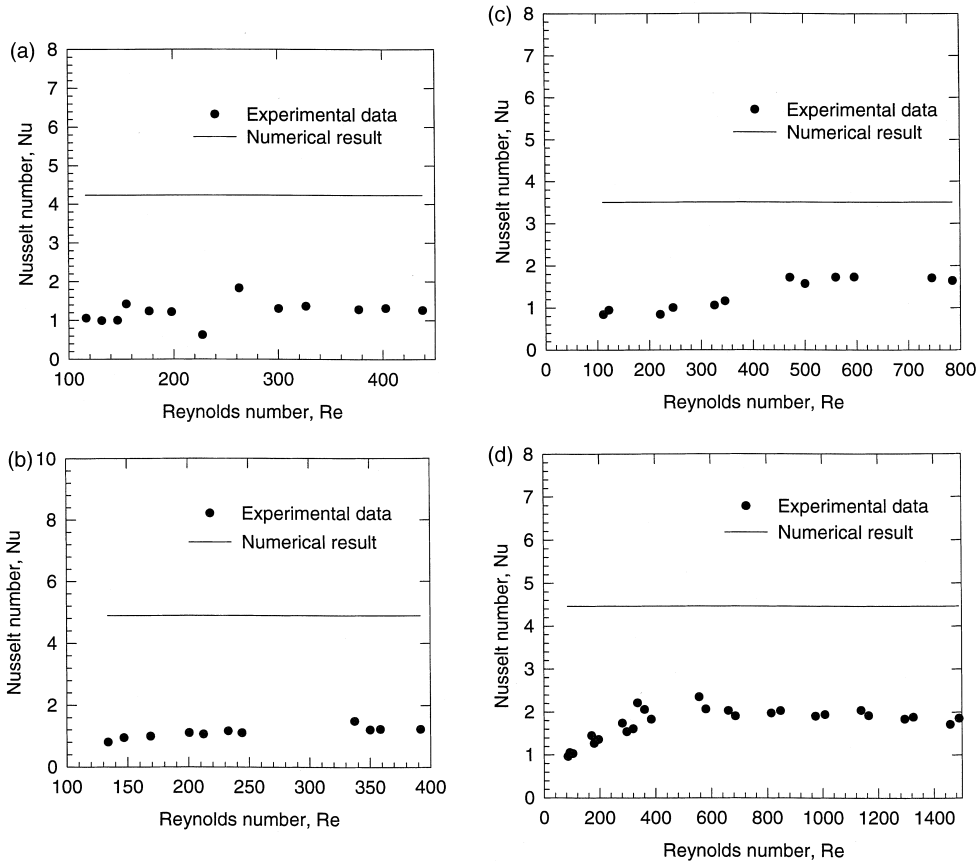

Fig. 7. A comparison of the experimentally determined Nusselt number versus Reynolds number with the results of the numerical analysis based on the conventional heat transfer theory. (a) $d_h = 62.3$ μm; (b) $d_h = 63.1$ μm; (c) $d_h = 114.5$ μm; (d) $d_h = 168.9$ μm.

trapezoidal microchannels similar to the ones used in this work. According to Qu et al. [13], the ratio of the roughness viscosity to the fluid viscosity in trapezoidal microchannels is proposed to take the following form:

$$\frac{\mu_R}{\mu} = A\,Re_k \times \frac{(R_h - l_{min})}{k}\left[1 - \exp\left(-\frac{Re_k}{Re}\frac{(R_h - l_{min})}{k}\right)\right]^2 \quad (24)$$

where A is given by

$$A = 5.8\left(\frac{R_h}{k}\right)^{0.35} \times \exp\left[Re^{0.94}\left(5.0\times10^{-5}\frac{R_h}{k} - 0.0031\right)\right]; \quad (25)$$

R_h is defined as the hydraulic radius of the microchannel, which is half of the channel hydraulic diameter d_h; l_{min} is the shortest distance from a point in the channel to the microchannel wall; Re_k denotes the local roughness Reynolds number and is defined as (Merkle et al. [6])

$$Re_k = \frac{W_k \rho_f k}{\mu_f} \quad (26)$$

where W_k denotes the velocity at the top of the roughness element and is given by (Merkle et al. [6])

$$W_k = \left(\frac{\partial w}{\partial n}\right)_\Gamma k \quad (27)$$

Eq. (24) implies [13] that the roughness viscosity μ_R has a maximum value near the wall and gradually diminishes as the distance from the wall increases. Because of this additional roughness viscosity near the wall, the velocity gradient near the wall should decrease. This is similar to the situation of cooling a

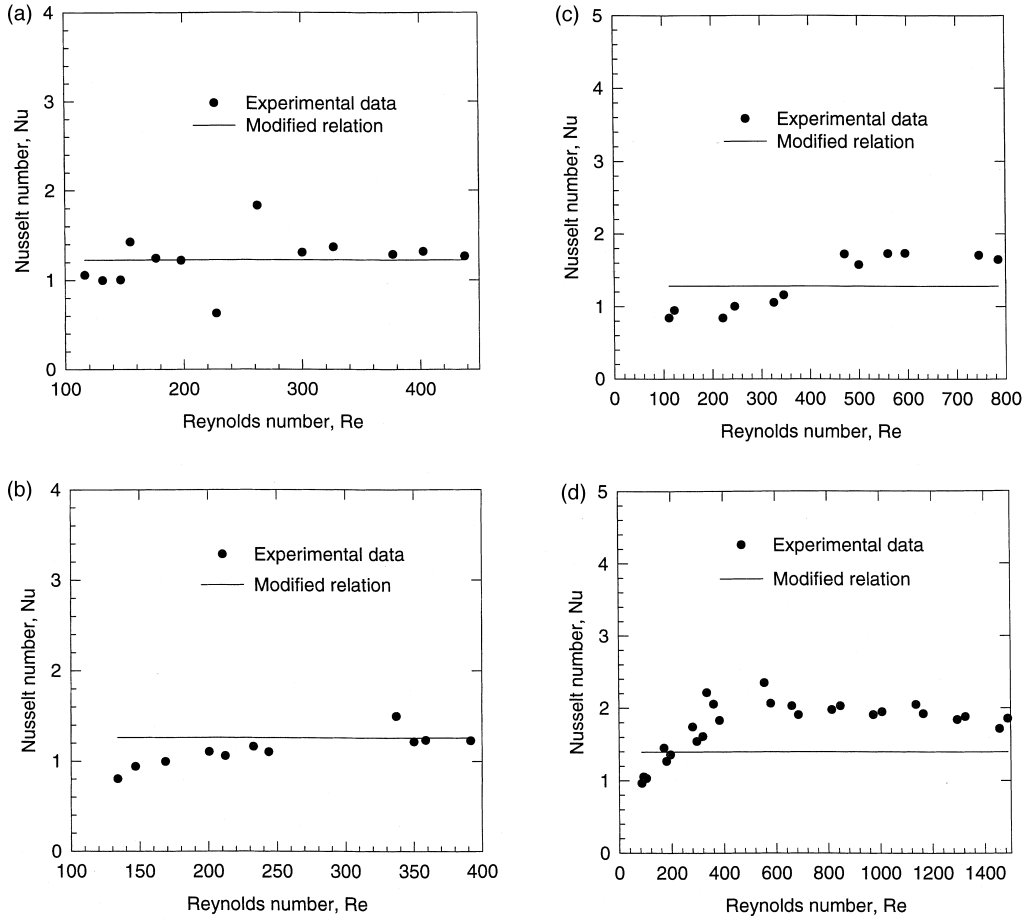

Fig. 8. A comparsion of experimentally determined Nusselt number versus Reynolds number with the predictions of the modified relationship, Eq. (28). (a) $d_h = 62.3$ μm; (b) $d_h = 63.1$ μm; (c) $d_h = 114.5$ μm; (d) $d_h = 168.9$ μm.

hot liquid by forcing the liquid to flow through a cold duct. Since for most liquids, the viscosity rises as the temperature falls, there will be a viscosity gradient in the liquid, with a high viscosity near the wall and a low viscosity away from the wall. This problem was discussed in details by McAdams [5] and Petukhov [10]. Consequently, in such a cooling process, the layers of the liquid near the wall will flow at a smaller velocity, or in other words, the velocity gradient near the wall will decrease.

The process of convective heat transfer always depends on the flow field. Generally, the change of the temperature gradient near the wall will be similar to the change of the velocity gradient near the wall. Since the velocity gradient near the wall is reduced because of the roughness viscosity, the temperature gradient near the wall is also reduced, and hence, the convective heat transfer is reduced. This may be the reason why the experimental Nusselt number is smaller than the numerical result of the conventional heat transfer theory.

Based on the discussion above, a modifying factor is proposed here which takes the surface roughness effect into account.

$$Nu_{\mathrm{R}} = Nu_{\mathrm{thy}}\left(\frac{\mu_{\mathrm{Rm}}}{\mu_{\mathrm{Rmw}}}\right) \tag{28}$$

where μ_{Rm} is the average roughness viscosity over a cross-section of the microchannel

$$\mu_{\mathrm{Rm}} = \frac{1}{A_{\mathrm{c}}}\int_{A_{\mathrm{c}}} \mu_{\mathrm{R}}\,\mathrm{d}A_{\mathrm{c}} \tag{29}$$

and μ_{Rmw} is the average roughness viscosity along the side and the bottom walls of the microchannel.

$$\mu_{\mathrm{Rmw}} = \frac{1}{A_w}\int_{A_w} \mu_{\mathrm{R}}\,\mathrm{d}A_{\mathrm{w}} \tag{30}$$

Fig. 8a and b show the comparison of the measured *Nu–Re* relationships with the predictions of the modified relation, Eq. (28). As can be seen from the figures, the curves predicted by the modified *Nu* relationship and the experimental results are in good agreements with each other. This implies that the roughness-viscosity model proposed in our previous work may be used to interpret the heat transfer characteristics in these microchannels.

4. Summary

The heat transfer characteristics of water flow in trapezoidal silicon microchannels is experimentally investigated. The results are compared with the numerical prediction based on the conventional heat transfer theory. It is found that the experimentally determined Nusselt number in microchannels is lower than that predicted by the numerical analysis. A roughness-viscosity model is applied in this paper to interpret the experimental results. Based on the roughness-viscosity model, a modified *Nu* relationship is proposed. A good agreement between the experimental data and the predictions from the modified relationship is found.

Acknowledgements

The authors wish to acknowledge the support from a Research Grant of the Natural Science and Engineering Research Council of Canada.

Appendix A. Experimental uncertainty analysis

According to Holman [3], if R is a given function of the independent variables $x_1, x_2, x_3, \ldots, x_n$, $R = R(x_1, x_2, x_3, \ldots, x_n)$, and $w_1, w_2, w_3, \ldots, w_n$ are the uncertainties in these independent variables, the uncertainty of R can be evaluated by

$$w_{\mathrm{R}} = \left[\left(\frac{\partial R}{\partial x_1}w_1\right)^2 + \left(\frac{\partial R}{\partial x_2}w_2\right)^2 + \cdots + \left(\frac{\partial R}{\partial x_n}w_n\right)^2\right]^{1/2} \tag{A1}$$

Eq. (22) can be further written as

$$\frac{w_{\mathrm{R}}}{R} = \left[\left(\frac{1}{R}\frac{\partial R}{\partial x_1}w_1\right)^2 + \left(\frac{1}{R}\frac{\partial R}{\partial x_2}w_2\right)^2 + \cdots + \left(\frac{1}{R}\frac{\partial R}{\partial x_n}w_n\right)^2\right]^{1/2} \tag{A2}$$

Based on the instruments and methods employed in our experiments, the uncertainties of our basic measured parameters are evaluated as follows

$$w_a = 0.8\ \mu\mathrm{m} \tag{A3a}$$

$$w_b = 0.8\ \mu\mathrm{m} \tag{A3b}$$

$$w_h = 0.8\ \mu\mathrm{m} \tag{A3c}$$

$$\frac{w_{L_3}}{L_3} = 0.01 \tag{A3d}$$

$$\frac{w_T}{T} = 0.008 \tag{A3e}$$

$$\frac{w_V}{V} = 0.02 \tag{A3f}$$

From Eqs. (A2)–(A3f), the uncertainties of some dependent parameters can be evaluated. For the hydraulic diameter of the microchannels,

$$d_h = \frac{4A_c}{P_c} \tag{A4a}$$

$$\frac{w_{d_h}}{d_h} = 0.0285 \tag{A4b}$$

For the heat removed by water,

$$Q = \rho_f c_{Pf} V(T_{out} - T_{in}) \tag{A5a}$$

$$\frac{w_Q}{Q} = 0.0611 \tag{A5b}$$

For the total area of the side and bottom walls of the microchannel

$$A_w = (2l + b) \cdot L_3 \tag{A6a}$$

$$\frac{w_{A_w}}{A_w} = 0.0359 \tag{A6b}$$

For the mean temperature difference between the water and the bottom wall of the microchannel plate,

$$\Delta T_m = \frac{1}{3}(T_1 + T_2 + T_3) - \frac{1}{2}(T_{in} + T_{out}) \tag{A7a}$$

$$\frac{w_{\Delta T_m}}{\Delta T_m} = 0.0365 \tag{A7b}$$

The above equations provides enough information to estimate the uncertainties of the final experimental results. The Reynolds number Re and Nusselt number Nu are related to the basic measured parameters by Eqs. (17) and (18). From Eq. (A2), their uncertainties are evaluated as

$$\frac{w_{Re}}{Re} = 0.046 \tag{A8a}$$

$$\frac{w_{Nu}}{Nu} = 0.085 \tag{A8b}$$

References

[1] T.M. Adams, S.I. Abdel-Khalic, S.M. Jeter, Z.H. Qureshi, An experimental investigation of single-phase forced convection in microchannels, Int. J. Heat Mass Transfer 41 (1998) 851–857.

[2] S.B. Choi, R.R. Barren, R.O. Warrington, Fluid flow and heat transfer in micro tubes, ASME DSC 40 (1991) 89–93.

[3] J.P. Holman, Experimental Methods for Engineers, 4th ed., McGraw-Hill, New York, 1984.

[4] G.M. Mala, D. Li, Flow characteristics of water in microtubes, International Journal of Heat and Fluid Flow 20 (1999) 142–148.

[5] W.H. McAdams, Heat Transmission, McGraw-Hill, New York, 1954.

[6] C.L. Merkle, T. Kubota, D.R.S. Ko, An analytical study of the effects of surface roughness on boundary-layer transition, AF Office of Scien. Res. Space and Missile Sys. Org., AD/A004786, 1974.

[7] S.V. Patankar, A numerical method for conduction in composite materials, flow in irregular geometries and conjugate heat transfer, in: Proceedings of 6th Int. Heat Transfer Conference, vol. 3, 1978, pp. 297–302.

[8] S.V. Patankar, Numerical Heat Transfer and Fluid Flow, Hemisphere, Washington, DC, 1980.

[9] X.F. Peng, G.P. Peterson, Convective heat transfer and flow friction for water flow in microchannel structures, Int. J. Heat Mass Transfer 39 (12) (1996) 2599–2608.

[10] B.S. Petukhov, Heat transfer and friction in turbulent pipe flow with variable physical properties, Advances in Heat Transfer 6 (1970) 504–564.

[11] R. Phillip, Micro-channel heat sinks, in: Advances in Thermal Modeling of Electronic Components, 2, ASME, New York, 1990 (Chapter 3).

[12] A.T. Prata, E.M. Sparrow, Heat transfer and fluid flow characteristics for an annulus of periodically varying cross section, 7 (1984) 285–304.

[13] W. Qu, G.Mm Mala, D. Li, Pressure-driven water flows in trapezoidal silicon microchannels, Int. J. Heat Mass Transfer 43 (2000) 353–364.

[14] I. Tani, Boundary layer transition, Annual Reviews of Fluid Mechanics, vol. 1, Annual Reviews Inc., Palo Alto, CA.

[15] D.B. Tuckerman, R.F.W. Pease, High-performance heat sinking for VLSI, IEEE Electron Device Letters EDL-2 (1981) 126–129.

[16] B. Wang, X. Peng, Experimental investigation on liquid forced-convection heat transfer through microchannels, Int. J. Heat Mass Transfer 37 (1994) 73–82.

[17] P.Y. Wu, W.A. Little, Measurement of friction factor for flow of gases in very fine channels used for micro-miniature Joule–Thompson refrigerators, Cryogenics 24 (8) (1983) 273–277.

[18] D. Yu, R. Warrington, R. Barron, T. Ameel, An experimental and theoretical investigation of fluid flow and heat transfer in microtubes, ASME/JSME Thermal Engineering Conference, vol. 1, pp. 523–530.

[19] G.M. Mala, Ph.D. Thesis, University of Alberta, 1999.